Chapter 16
Predicting Urban Heat Island Mitigation with Random Forest Regression in Belgian Cities

Mitali Yeshwant Joshi, Daniel G. Aliaga, and Jacques Teller

Abstract An abundance of impervious surfaces like building roofs in densely populated cities make green roofs a suitable solution for urban heat island (UHI) mitigation. Therefore, we employ random forest (RF) regression to predict the impact of green roofs on the surface UHI (SUHI) in Liege, Belgium. While there have been several studies identifying the impact of green roofs on UHI, fewer studies utilize a remote-sensing-based approach to measure impact on Land Surface Temperatures (LST) that are used to estimate SUHI. Moreover, the RF algorithm, can provide useful insights. In this study, we use LST obtained from Landsat-8 imagery and relate it to 2D and 3D morphological parameters that influence LST and UHI effects. Additionally, we utilise parameters that influence wind (e.g., frontal area index). We simulate the green roofs by assigning suitable values of normalised difference-vegetation index and built-up index to the buildings with flat roofs. Results suggest that green roofs decrease the average LST.

Keywords Green roofs · Random forest regression · Urban heat island (UHI) · Land surface temperature (LST)

16.1 Introduction

Unprecedented urban growth has led to increased building densities resulting in limited green spaces in cities, exacerbating the impacts of climate change (Dong et al. 2020; Wang et al. 2022). Consequently, urban areas are experiencing higher

M. Y. Joshi (✉) · J. Teller
LEMA Research Group, Urban & Environmental Engineering Department, University of Liège, Liege, Belgium
e-mail: mjoshi@uliege.be

J. Teller
e-mail: Jacques.Teller@uliege.be

D. G. Aliaga
Department of Computer Science, Purdue University, West Lafayette, IN, USA
e-mail: aliaga@cs.purdue.edu

R. Goodspeed et al. (eds.), *Intelligence for Future Cities*, The Urban Book Series,
https://doi.org/10.1007/978-3-031-31746-0_16

temperatures as compared to rural regions, which is known as the urban heat island (UHI) effect (Stewart and Oke 2012; Santamouris 2013). Negative impacts of UHI effect include increased energy consumption, carbon emissions, decreased comfort levels, and global warming (Bowler et al. 2010). Thus, to circumvent these impacts, identifying solutions to mitigate the UHI effect is crucial.

The UHI phenomenon is primarily caused by a high density of built-up areas, as well as low albedo of urban surfaces, resulting in absorption of excess solar radiation (Razzaghmanesh et al. 2016). In this scenario, green roofs are highly relevant owing to the abundance of building rooftops made of impervious surfaces in cities (Francis and Jensen 2017; Joshi and Teller 2021). Green roofs prevent the absorption of short-wave radiation and act as thermal insulators (Razzaghmanesh et al. 2016). Green roofs also prevent heat from entering the structures in summer, reducing energy consumption (di Giuseppe and D'Orazio 2014). Moreover, green roofs also increase evapotranspiration and natural ventilation within built-up areas (Li et al. 2014). Along with this, green roofs also have other benefits in terms of biodiversity and runoff retention. Thus, considering their multifold benefits, green roofs are a suitable strategy for UHI mitigation (Jamei et al. 2021).

Researchers have analyzed green roofs and their impact using numerous methods. Most of the studies use numerical modelling, simulations and statistical analysis to analyze greening scenarios (Bartesaghi Koc et al. 2018). However, micro-scale urban canopy models (UCM) and microclimate simulation models like ENVImet cannot be employed for entire city due to computational demands (Mirzaei, 2015; Lin et al. 2021). While mesoscale models like weather research and forecasting (WRF) coupled with UCM aid in conducting research at a regional scale, running these models at high resolution require significant computational resources. Therefore, most of the WRF studies are carried out at a resolution of 1 km (Yang and Bou-Zeid 2019; Wang et al. 2022). Moreover, analyzing and processing these models are generally challenging for most urban planners (Lin et al. 2021). Therefore, remote sensing approach can be advantageous as finer resolution datasets are increasingly available. Furthermore, the analysis using remote sensing can be straightforward with existing geographic information system (GIS) softwares like QGIS and ArcGIS for urban practitioners (Bartesaghi Koc et al. 2018; Lin et al. 2021).In this study, we employ a remote sensing-based approach for analyzing the impact of green roofs on UHI.

Traditionally, UHI effect is classified into surface and air UHI, referring to the surface and air temperature respectively (Roth et al. 1989; Kleerekoper et al. 2012; Kim and Brown 2021). The impact of Green roofs on air temperature is debatable, however, their impact on surface temperature is significant (Berardi et al. 2014; Francis and Jensen 2017). Thus, we focus mainly on the impact of green roofs on surface temperature. This estimate, referred to as Land Surface Temperature (LST) is obtained using satellite images.

UHI effect is the outcome of dynamic interactions between the macroclimate and urban morphology (Boccalatte et al. 2020). Thus, along with greening, several other morphological parameters influence LST. The relationship of LST with several morphological parameters has been investigated using satellite data (El-Zeiny and

Effat 2017). For example, the Normalised difference vegetation index (NDVI) has a strong to moderate negative correlation with LST, whereas normalized difference built-up index (NDBI) has a positive correlation (Adeyeri et al. 2017; Govil et al. 2020). Parameters such as building densities also influence LST. 3D data was also strongly influencing LST in some studies (Zha et al. 2010). Moreover, detailed 3D parameters such as frontal area index (FAI) and sky view factor (SVF), can be now computed in a raster format for facilitating a better analysis (Asadi et al. 2020). Subsequently, 3D parameters can represent the contribution of shadows, solar radiation and orientation.

The relationship between LST and related parameters have been previously analyzed using ordinary least square (OLS) regression and graphically weighted regression (Deilami et al. 2018). Recent studies also have used machine learning in predicting changes in LST (Jato-Espino et al. 2022; Lyu et al. 2022). For example, Asadi et al. (2020) use Artificial neural network (ANN) to predict changes in LST after implementing green roofs in Austin, Texas. Their study showed that LST decreased by 1.96 degree Celsius on an average after greening 3.2% of the roofs. The study used 2D and 3D urban morphological parameters in their analysis. Although the parameters are comprehensive for the task, parameters influencing wind flow, such as frontal area index (FAI) could have enhanced the analysis (Wang et al. 2021). Moreover, random forest (RF) regression has proven to be robust in predicting several scenarios (Jato-Espino et al. 2022; Lyu et al. 2022). Along with this, RF regression prediction is regarded as being unaffected by the multicollinearity and distribution of data (Matsuki et al. 2016; Busato et al. 2023). Thus, in this study, we explore the performance of RF regression in predicting changes in LST caused by green roofs.

16.2 Methodology

Figure 16.1 represents the broad methodology used in this study.

16.3 Study Area and Dataset

In this study, we analyze the Brussels capital region and the city of Liege in Belgium. Brussels is the capital of Belgium and has an area of 161.4 km^2 with around 1,222,637 inhabitants (Christis et al. 2019). As it is the national capital, it is highly dense and compact with limited space for developing green infrastructure within the city. Liege, on the other hand, is located in the Wallonia region of Belgium. The city is the third largest city in terms of population in the country, with an area of 69 km^2 and 196,296 inhabitants. The city is highly compact with significant building density in the center and open residential areas in the outskirts (Joshi et al. 2022). Thus, roof greening is a suitable UHI mitigation strategy for both cities.

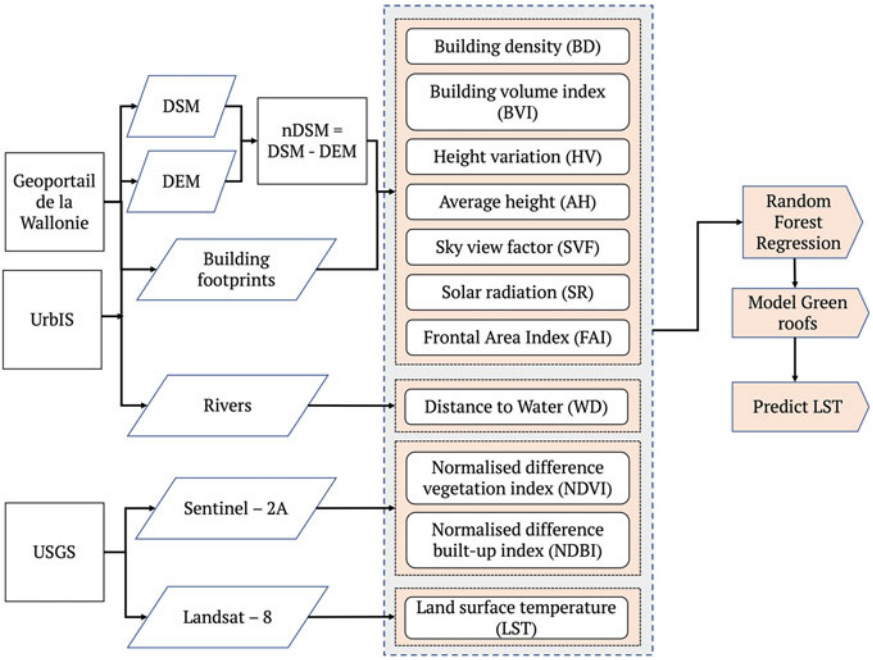

Fig. 16.1 Methodology

We use four datasets mainly for computing the parameters influencing LST. Table 16.1 presents the dataset used and respective sources for Liege and Brussels.

We processed all rasters to 30 m resolution as it is the resolution of LST obtained from Landsat-8.

Table 16.1 Datasets used for analysis with their respective sources for Liege and Brussels

Datasets	Liege	Brussels
Building footprints	PICC (Projet Informatique de Cartographie Continue) dataset, with an accuracy of less than 25 cm	The footprints are obtained from UrbIS online (data platform for Brussels capital region)
Building heights	Digital surface model (DSM) and the digital elevation model (DEM)	3D model of Brussels from UrbIS
LST	Landsat-8 level 1 image captured on July 18, 2021	
NDVI and NDBI	Sentinel-2 multispectral image obtained on 21st July 2021	

16.4 Parameters Influencing LST

16.4.1 Building Density

To obtain building density (BD), we first transform the building footprints to a raster with 1 m resolution. Thereafter, we aggregate the raster by summing the building pixels to a raster with 30 m resolution, representing building density. Thus, building density is computed as:

$$BD = \sum_{i=1}^{n} a_i \tag{16.1}$$

where a_i is the 1 by 1 m pixel covered by building and n is the total number of 1 m pixels in 30 m pixel.

16.4.2 Building Volume Index

Building volume index (BVI) is the building volume in a pixel and it is calculated as follows:

$$BVI = \sum_{i=1}^{n} a_i \times h_i \tag{16.2}$$

where a_i is the 1 m pixel covered by building, h_i is the height of the building in the 1 m pixel and n is the total number of 1 m pixels in 30 m pixel.

16.4.3 Sky View Factor

Sky view factor (SVF) is the ratio of proportion of sky visible from the ground at a given position, to the proportion of sky not obstructed by the surrounding built-up (Rodler and Leduc 2019). We calculate it with the Relief Visualisation Toolbox of QGIS 3 (Zakšek et al. 2011; Kokalj and Somrak 2019).

We use the DSM and the building footprint dataset to generate the raster with building height information. We consider open spaces and roads along with the bottom of the buildings at 0 m. We consider a search radius of 100 m and the number of directions as 16 for SVF calculation (Dirksen et al. 2019). We compute SVF at a resolution of 1 m and later resample it at 30 m resolution.

16.4.4 Solar Radiation

The amount of solar radiation (SR) received by the surfaces in the city influences the LST (Bristow and Campbell 1984; Asadi et al. 2020). Therefore, we compute the SR using the solar radiation tool in ArcGIS Pro 2.9.1. This represents the global radiation, which is the total incoming solar radiation and is calculated for each pixel of DSM. The value of SR was calculated on July 18, 2021 to match the date of acquisition for Landsat-8 image.

16.4.5 Normalized Difference Vegetation Index (NDVI)

NDVI is used to detect bare soil and vegetation (Montandon and Small 2008; Ferreira and Duarte 2019). In a way, it represents the pervious regions in the city. We calculate the NDVI using the Sentinel-2A satellite imagery captured on July 21, 2021, from the United States geological survey (USGS) (https://earthexplorer.usgs.gov/). We chose the image on this date as July and August experience higher temperatures. Moreover, among the images available for this time frame, the selected image had the lowest and most acceptable cloud coverage of less than one per cent. Sentinel-2A image is of 10 m spatial resolution and thus the NDVI obtained is also at 10 m. We calculate NDVI using the near infrared (NIR) and red (R) bands of the image as follows:

$$NDVI = \frac{NIR - R}{NIR + R} \tag{16.3}$$

16.4.6 Normalized Difference Built-Up Index (NDBI)

Zha et al. (2010) defined NDBI to determine urban and built-up areas. It is used to express the intensity of urbanization (Chen et al. 2006). Although we use building density, we consider NDBI as one of the parameters as it helps highlight other urban areas that are not buildings. Moreover, it also explains the development intensity by indicating impervious surfaces. We calculate NDBI using the Sentinel-2A image used for obtaining NDVI. To compute NDBI, we need short wave infrared (SWIR) band, which has a resolution of 20 m and NIR with a resolution of 10 m. Therefore, the SWIR band was resampled to 10 m resolution for the calculation. NDBI is thus calculated as follows:

$$NDBI = \frac{SWIR - NIR}{SWIR + NIR} \tag{16.4}$$

16.4.7 Frontal Area Index (FAI)

FAI influences the wind flow, thus influencing the LST. It is defined as the area of building walls facing the wind flow in a particular direction (Wong et al. 2010). We compute FAI using the methodology of H. Li et al. (2021) in this paper. The method involves rasterization of the building height and area and computing the FAI at 30 m resolution. The FAI is only calculated for northerly/easterly winds.

16.4.8 Height Variation (HV)

Height Variation (HV) is the variation observed in building heights (1 m pixel) in 30 m pixel. For computing HV, we first transform building heights to a 1 m raster. Then, we aggregate the raster to 30 m with standard deviation of heights in a 30 m pixel using geopandas package in python 3.

16.4.9 Average Height (AH)

Similar to HV, we compute average height (AH) for the pixels by aggregating 1 m height pixels to 30 m, by averaging the heights of 1 m pixels.

16.4.10 Distance to Water

Liege city is situated on the banks of river Meuse. The river divides the city into two parts. Similarly, Brussels has the river Senne that flows through the region. As water bodies have a significant impact on surface temperature (Wu and Zhang 2018), we consider this parameter in our analysis. We obtained the river shapefiles for Liege and Brussels fro, geoportail of Wallonia and UrBIS respectively. We calculate this parameter using Euclidean distance tool to the river shapefiles at 30 m resolution.

16.5 Land Surface Temperature (LST)

We calculate the LST using the Landsat-8 level 1 image captured on 18th July 2021. We choose the image on this date since July and August experience higher temperatures. Moreover, the image on this date had the lowest and most acceptable cloud coverage of less than one per cent. We use the thermal band 10 to compute the LST (in Kelvin (K)) using the following equations (USGS 2019).

$$L_\lambda = M_L Q_{cal} + A_L \tag{16.5}$$

where L_λ = TOA (Top of Atmosphere) spectral radiance (Watts/(m^2 * srad * μm)), M_L = Band-Specific multiplicative rescaling factor from the metadata, A_L = Band-specific additive rescaling factor from the metadata, Q_{cal} = Quantized and calibrated standard product pixel values (DN)

$$T = \frac{K_2}{lnln\left(\frac{K_1}{L_\lambda} + 1\right)} \tag{16.6}$$

where T = TOA brightness temperature (K), K_1 = Band-specific thermal conversion constant from the metadata, K_2 = Band-specific thermal conversion constant from the metadata. We further convert the LST values to degrees Celsius (°C).

16.6 Data Processing

We first generate random points in ArcGIS Pro 2.9.1 over the Brussels capital region and Liege city with 100 m spacing between the points to avoid spatial autocorrelation. We consider 100 m as minimum distance as spatial variability of urban temperatures is around 100 m (Bechtel et al. 2015; Li et al. 2021; Hereher et al. 2022). We then use the "*extract values to point*" tool, to extract values of all the parameters mentioned above to the randomly generated points. We obtain 7500 points in Brussels and 4000 points in Liege, giving us a total of 11,500 points for training and testing the RF regression model.

16.7 RF Regression

RF is a supervised machine learning algorithm proposed by Breiman (2001). The RF regression algorithm combines a large set of regression trees, where dataset is broken down into smaller subsets to predict a response variable by learning decision rules (Breiman et al. 1984). The trees are combined using bootstrap aggregation or bagging, such that each set is run independently, and the outputs are merged to achieve an accurate prediction (Breiman 1996).

The regression begins by selecting n samples of k random observations from a training dataset. Then, individual decision trees are built for each sample. These n trees are run in parallel, and separate outputs are generated. The mean of these outputs results in the final prediction. The random selection in RF regression prevents overfitting (Huynh-Thu and Geurts 2019).

In this study, RF regression is implemented in python through the scikit-learn package. The package includes several parameters that can be tuned for an improved

performance. We focus on tuning the number of trees (*ntree*) and number of features randomly sampled at each split (*mtry*).

RF regression is a supervised and straightforward method, which is fast and robust to the noise in the data (Kontschieder et al. 2011; Izquierdo-Verdiguier and Zurita-Milla 2020). We train the RF regressor model using 80% of the data points and test it over remaining 20% of the data points. We validate the RF regression model with *k*-fold cross validation, with *k* set at five. Additionally, we identify the suitable *mtry* and *ntree* based on the lowest value of RMSE (root mean squared error). We also analyse the R-squared value of the relation between observed and predicted LST for both the cities to understand the goodness of fit.

16.8 Simulating Green Roofs

We simulate the green roofs similar to the method proposed by Asadi et al. (2020). Liege has around 20% of flat roofs as computed in the study by Joshi et al. (2020). For Brussels, we identify flat roofs using the 3D model of the region available at UrbIS online. As it will be unrealistic to simulate green roofs on all of these buildings, we consider buildings with area larger than 100 m^2 to be suitable for greening in this study. Figure 16.2 shows the potential roofs in Brussels and Liege. Around 92,333 roofs (out of 256,484) in Brussels are flat, whereas 23,326 roofs (out of 136,170) are flat in Liege.

Green roofs are of mainly of two types: extensive and intensive green roofs. The third type of green roof is a green roof somewhere in between the two main types.

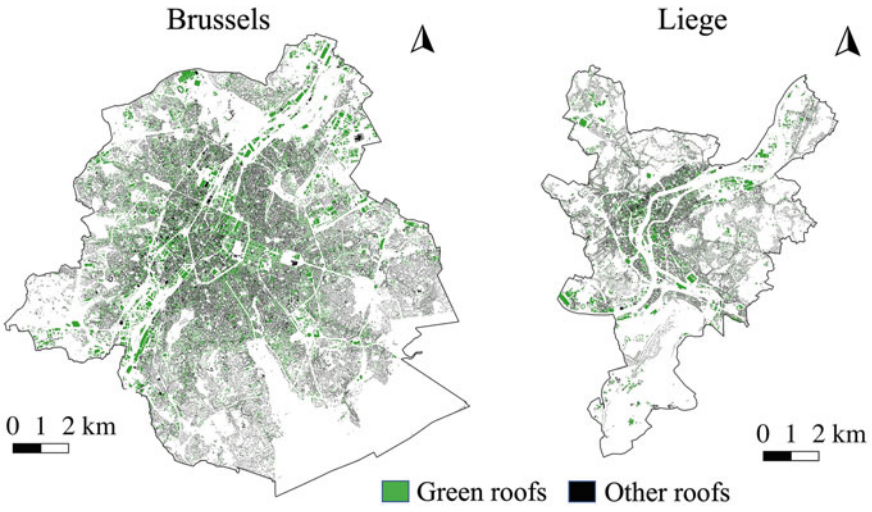

Fig. 16.2 Potential roofs for greening in both the cities

Extensive green roofs have relatively thinner substrate vegetation compared to the intensive ones. Intensive green roofs have a thick substrate layer and dense vegetation, such as rooftop gardens and agriculture (Joshi and Teller 2021). We simulate green roofs by changing the value of NDVI and NDBI for the potential roofs in both cities.

The NDVI values for green surfaces vary from 0.3 to 1 depending upon the intensity of greening. However, for green roofs, NDVI values range from 0.3 to 0.8, considering the range from extensive to intensive green roofs. Further, changing NDBI values also becomes mandatory due to the change in NDVI. We change NDBI values according to the relationship derived between original NDVI and NDBI values obtained from Sentinel-2 for Brussels and Liege. Figure 16.3 represents this correlation.

The relation between NDBI and NDVI is significant, given that the R-squared value is 0.87 and pearson correlation co-efficient is less than 0.05. Based on this relation, Table 16.2 provides the corresponding values of NDBI for each NDVI from 0.3 to 0.8.

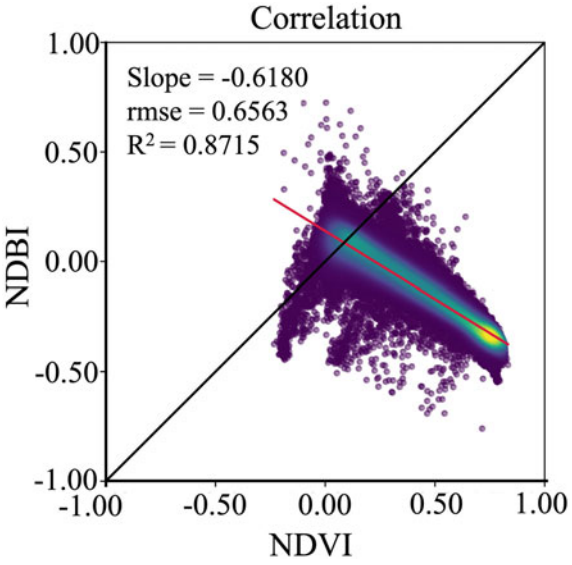

Fig. 16.3 Correlation between NDVI and NDBI values

Table 16.2 Values of NDBI corresponding to NDVI values of green roofs

NDVI (x)	NDBI(y)
0.3	−0.05474677
0.4	−0.11654956
0.5	−0.17835235
0.6	−0.24015514
0.7	−0.30195793
0.8	−0.36376072

Wherever there is a potential roof with 100 m^2, we convert the pixels to NDVI values indicated in the table. We do this by first resampling the 10 m NDVI to 1 m spatial resolution. Thereafter, we change the values of NDVI at the pixels corresponding to building footprints of potential roofs. Later, we aggregate the NDVI with green roofs to 30 m spatial resolution by calculating the average value. Similarly, we convert the NDBI values of potential green roofs to the values in Table 16.1 corresponding to the respective NDVI values. Thus, we generate predictions for six scenarios for six values of NDVI and NDBI in Table 16.1. As only the roof is converted to a "green roof", we keep other building related parameters unchanged. We run the trained model on the newly built NDVI and NDBI along with other variables and predict changes in LST.

16.9 Results

16.9.1 Model Results and Accuracy

Figure 16.4 shows the results of RF hyperparameters (*mtry* and *ntree*). We did the optimization based on RMSE. Results indicate that RF hyperparameters affect prediction accuracy only by 0.02 °C. The optimal results are observed at *ntree* = 6000 and *mtry* = 3, with lowest RMSE (1.65 °C).

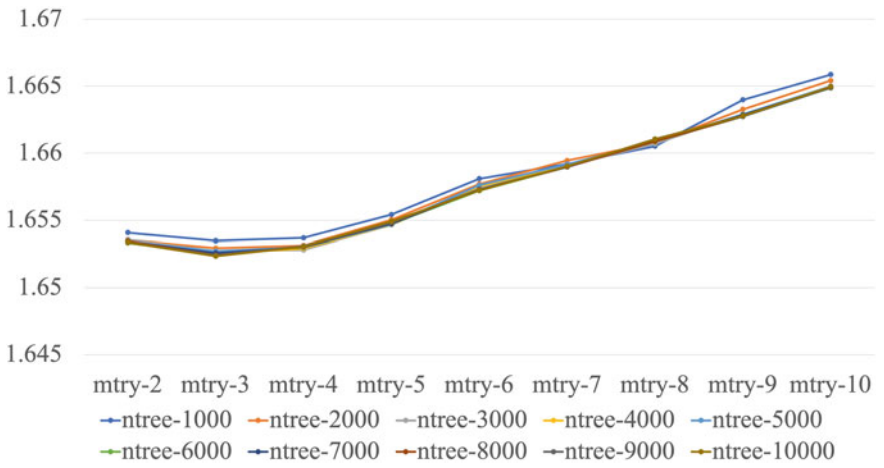

Fig. 16.4 Optimisation of hyperparameters *ntree* and *mtry*

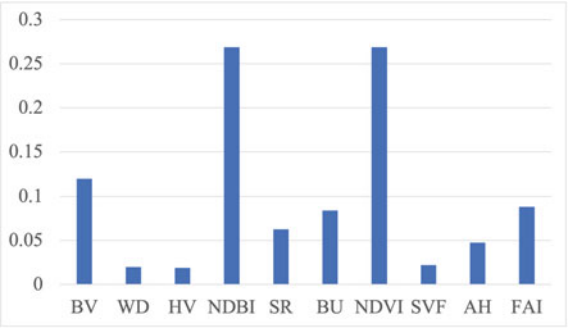

Fig. 16.5 Feature importance of the optimised model

16.9.2 Variable Importance at Optimal Ntree *and* Mtry

Figure 16.5 shows feature importance in an optimized RF regression model. We observe that NDBI and NDVI are the most important parameters, followed by BVI, FAI, AH, SVF, HV and WD.

The model is mainly driven by NDBI, NDVI, BVI and FAI values, which decide the value of LST.

16.9.3 Comparing Predicted and Observed Values of LST

Here, we compare the predicted values of LST with the observed values of LST from Landsat-8 for both the cities. The city of Brussels has observed values of LST ranging from 21 to 42 °C, whereas the city of Liege has the values of LST ranging from 18 to 38 °C (Fig. 16.6). The predicted values for both the cities, however, fall between 21 and 33 °C (Fig. 16.7).

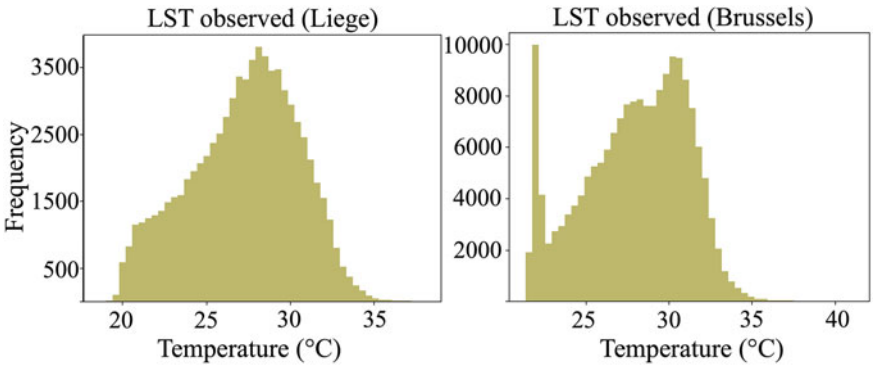

Fig. 16.6 Distribution of observed LST values for Liege and Brussels

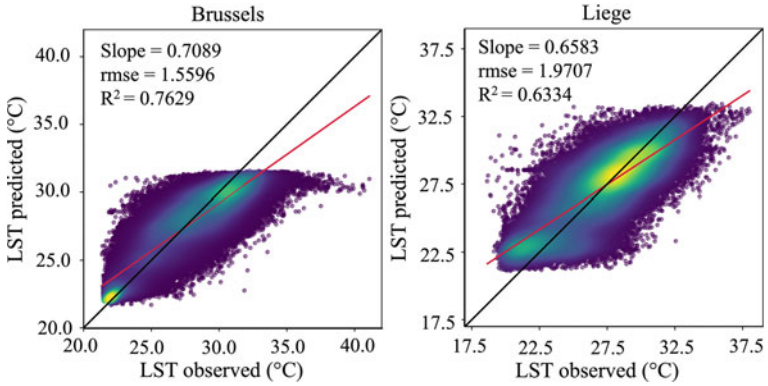

Fig. 16.7 Comparison of predicted vs observed values of LST for Brussels and Liege

We observe that the trained model's R-squared value is 0.76 with an RMSE of 1.55 °C for Brussels. For Liege, the R-squared value is 0.633 with an RMSE of 1.97 °C (Fig. 16.7). We observe that the values between 21 and 33 °C are predicted more accurately compared to the values outside of this range (Fig. 16.7). The reason could be the distribution of data which ranges from 19 to 38 °C, with 80% of the points in the range between 21 and 33 °C. As the model tends to slightly underpredict LST, we compare the effect of green roofs on LST with the predicted LST of our model, to understand the actual impact green roofs can have on LST.

16.9.4 Prediction After Green Roofs

Based on the model, after adding intensive green roofs (NDVI = 0.8) to potential buildings, average LST is shown to be reduced by 0.67 °C and 0.46 °C in Liege, whereas average LST is shown to be reduced by 0.68 and 0.48 °C in the Brussels capital region in building area and entire city respectively. On the other hand, when extensive green roofs (NDVI = 0.3) are added to potential buildings, the average LST can reduce by 0.32 °C and 0.36 °C in Liege, and the average LST can reduce by 0.22 and 0.26 °C in the Brussels capital region in building area and entire city respectively. Figure 16.8 shows the predicted LST for each green roof scenario ranging from NDVI of 0.3–0.8.

Figure 16.9 depicts the distribution of pixels in each class of LST. With increase in NDVI value corresponding to green roofs, there is a decrease in pixels within the range of 32–35 °C for Liege as well as Brussels.

Similarly, Fig. 16.10 depicts the spatial variation in LST with adding intensive and extensive green roofs. As observed in Fig. 16.8, with increase in NDVI values of green roofs, we observe a reduction in pixels with temperature ranges between 29 and 35 °C.

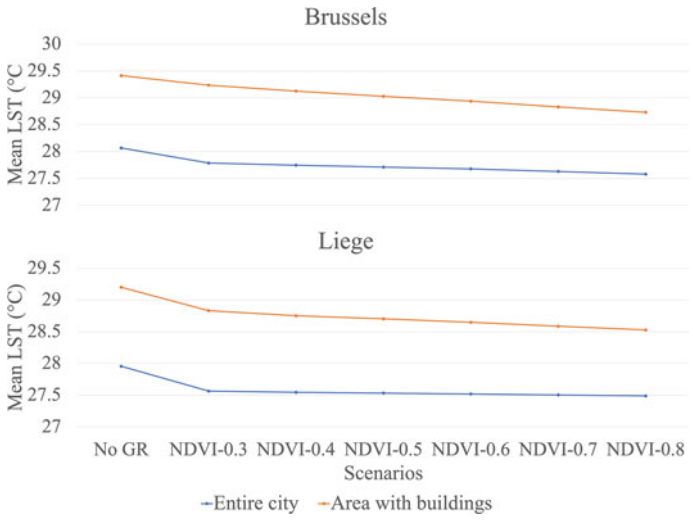

Fig. 16.8 Mean of predicted LST in Liege and Brussels for different scenarios

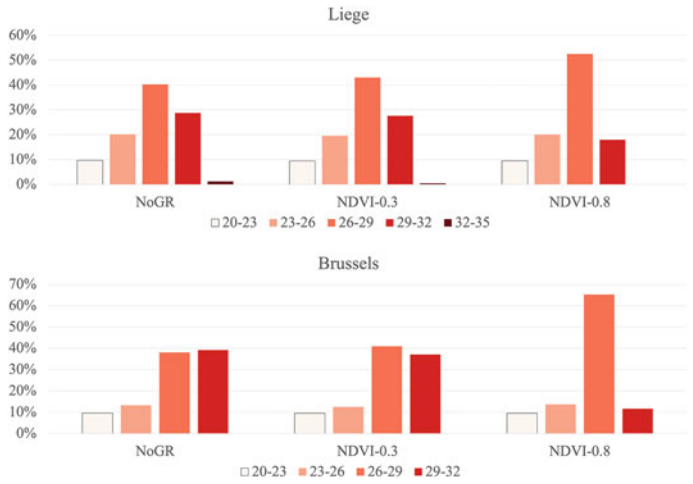

Fig. 16.9 Distribution of proportion of pixels in LST ranges

16.10 Discussion and Conclusions

In this study, we explore the RF regressor model for predicting impact of green roofs on LST. When comparing the observed LST with predicted LST, the model shows a significant goodness of fit. The RF model suggests that green roofs have potential to reduce LST. The benefit of green roofs is higher with intensive green roofs as compared to extensive green roofs.

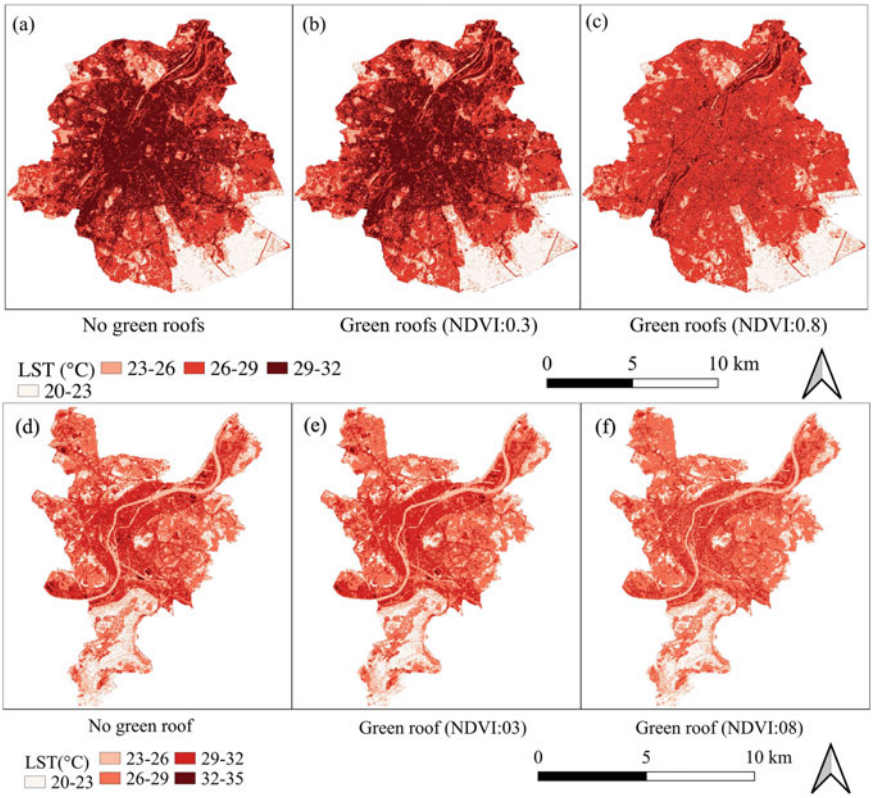

Fig. 16.10 Differences in LST in Brussels and Liege city for different greening scenarios

Although the impact of green roofs on LST on an average seems to be smaller, it is significant in terms of number of pixels where we observe the reduction of temperature (Fig. 16.9). However, small changes in LST may also indicate that when green roofs are placed on existing potential roofs, the impact may not be very significant (at least in case of extensive type of green roofs).

The prediction of LST depends on the training of the RF regressor model. Therefore, we include the data from two major cities in Belgium namely, Brussels and Liege, in order to have sufficient data points for training. However, we observe that the model does not perform well to predict extreme temperatures. To overcome this issue, adding more cities to the dataset can improve prediction accuracy.

Apart from this, the parameter importance of the model implies that NDVI, NDBI and BV govern the predictions. Importance of other parameters such as SVF, WD and HV are relatively low, yet theyare known to be important predictors of the UHI effect (Rodler and Leduc 2019). A reason could be multi-collinearity within the variables. As multi-collinearity does not affect predictions, we consider all the variables to capture maximum variance in the model. For understanding the feature importance,

it is important to drop the variables causing multi-collinearity. Further research can combine RF regressor with principal component analysis (PCA) to enhance this analysis.

In this study, we include data points all over the city. However, splitting the training samples into built-up area and non-built up with added cities can improve the prediction accuracy of the model. Additionally, further research can also focus just on analyzing only the built-up area of several cities.

Current model only considers changes in NDVI and NDBI to simulate green roofs. As greening can influence neighborhood areas as well, addition of a neighborhood effect in the model can also increase the prediction accuracy of the model.

Lastly, use of RF regression in prediction of changes in LST after introducing green roofs in a city is a novel and a promising approach, given the proven robustness of RF algorithm in several studies. The model successfully indicates the potential of greening the roofs for reducing the LST in cities. Asadi et al. (2020) performed a similar study using ANN model for Austin, Texas. However, in this study, we introduced two additional parameters influencing wind flow, FAI and HV. We see that FAI influences the model, however, HV has the lowest impact.

References

Adeyeri OE, Akinsanola AA, Ishola KA (2017) Investigating surface urban heat island characteristics over Abuja, Nigeria: relationship between land surface temperature and multiple vegetation indices. Remote Sens Appl 7:57–68. https://doi.org/10.1016/J.RSASE.2017.06.005

Asadi A, Arefi H, Fathipoor H (2020) Simulation of green roofs and their potential mitigating effects on the urban heat island using an artificial neural network: a case study in Austin, Texas. Adv Space Res 66:1846–1862. https://doi.org/10.1016/J.ASR.2020.06.039

Bartesaghi Koc C, Osmond P, Peters A (2018) Evaluating the cooling effects of green infrastructure: a systematic review of methods, indicators and data sources. Sol Energy 166:486–508. https://doi.org/10.1016/J.SOLENER.2018.03.008

Bechtel B, Alexander PJ, Böhner J, et al (2015) Mapping local climate zones for a worldwide database of the form and function of cities. ISPRS Int J Geo-Inform 4:199–219. https://doi.org/10.3390/IJGI4010199

Berardi U, GhaffarianHoseini AH, GhaffarianHoseini A (2014) State-of-the-art analysis of the environmental benefits of green roofs. Appl Energy 115:411–428. https://doi.org/10.1016/J.APENERGY.2013.10.047

Boccalatte A, Fossa M, Gaillard L, Menezo C (2020) Microclimate and urban morphology effects on building energy demand in different European cities. Energy Build 224:110129. https://doi.org/10.1016/j.enbuild.2020.110129

Bowler DE, Buyung-Ali L, Knight TM, Pullin AS (2010) Urban greening to cool towns and cities: a systematic review of the empirical evidence. Landsc Urban Plan 97:147–155. https://doi.org/10.1016/J.LANDURBPLAN.2010.05.006

Breiman L, Friedman JH, Olshen RA, Stone CJ (1984) Classification and regression trees. CRC Press

Breiman L (1996) Bagging predictors. Mach Learn 24:123–140. https://doi.org/10.1007/BF00058655

Breiman L (2001) Random forests. Mach Learn 45:5–32. https://doi.org/10.1023/A:1010933404324

Bristow KL, Campbell GS (1984) On the relationship between incoming solar radiation and daily maximum and minimum temperature. Agric for Meteorol 31:159–166. https://doi.org/10.1016/0168-1923(84)90017-0

Busato S, Gordon M, Chaudhari M et al (2023) Compositionality, sparsity, spurious heterogeneity, and other data-driven challenges for machine learning algorithms within plant microbiome studies. Curr Opin Plant Biol 71:102326. https://doi.org/10.1016/J.PBI.2022.102326

Chen X-L, Zhao H-M, Li P-X, Yin Z-Y (2006) Remote sensing image-based analysis of the relationship between urban heat island and land use/cover changes. Remote Sens Environ 104:133–146. https://doi.org/10.1016/j.rse.2005.11.016

Christis M, Athanassiadis A, Vercalsteren A (2019) Implementation at a city level of circular economy strategies and climate change mitigation—the case of Brussels. J Clean Prod 218:511–520. https://doi.org/10.1016/J.JCLEPRO.2019.01.180

Deilami K, Kamruzzaman M, Liu Y (2018) Urban heat island effect: a systematic review of spatio-temporal factors, data, methods, and mitigation measures. Int J Appl Earth Obs Geoinf 67:30–42. https://doi.org/10.1016/J.JAG.2017.12.009

di Giuseppe E, D'Orazio M (2014) Assessment of the effectiveness of cool and green roofs for the mitigation of the Heat Island effect and for the improvement of thermal comfort in Nearly Zero Energy Building. 58:134–143. https://doi.org/10.1080/00038628.2014.966050

Dirksen M, Ronda RJ, Theeuwes NE, Pagani GA (2019) Sky view factor calculations and its application in urban heat island studies. Urban Clim 30:100498. https://doi.org/10.1016/J.UCLIM.2019.100498

Dong J, Lin M, Zuo J et al (2020) Quantitative study on the cooling effect of green roofs in a high-density urban area—a case study of Xiamen, China. J Clean Prod 255:120152. https://doi.org/10.1016/J.JCLEPRO.2020.120152

El-Zeiny AM, Effat HA (2017) Environmental monitoring of spatiotemporal change in land use/land cover and its impact on land surface temperature in El-Fayoum governorate, Egypt. Remote Sens Appl 8:266–277. https://doi.org/10.1016/J.RSASE.2017.10.003

Ferreira LS, Duarte DHS (2019) Exploring the relationship between urban form, land surface temperature and vegetation indices in a subtropical megacity. Urban Climate 27:105–123. https://doi.org/10.1016/J.UCLIM.2018.11.002

Francis LFM, Jensen MB (2017) Benefits of green roofs: a systematic review of the evidence for three ecosystem services. Urban for Urban Green 28:167–176. https://doi.org/10.1016/J.UFUG.2017.10.015

Govil H, Guha S, Diwan P et al (2020) Analyzing linear relationships of LST with NDVI and MNDISI using various resolution levels of landsat 8 OLI and TIRS data. Adv Intell Syst Comput 1042:171–184. https://doi.org/10.1007/978-981-32-9949-8_13/TABLES/5

Hereher M, Eissa R, Alqasemi A, el Kenawy AM (2022) Assessment of air pollution at Greater Cairo in relation to the spatial variability of surface urban heat island. Environ Sci Pollut Res 29:21412–21425. https://doi.org/10.1007/S11356-021-17383-9/FIGURES/10

Huynh-Thu VA, Geurts P (2019) Unsupervised gene network inference with decision trees and random forests. Methods Mol Biol 1883:195–215. https://doi.org/10.1007/978-1-4939-8882-2_8/COVER

Izquierdo-Verdiguier E, Zurita-Milla R (2020) An evaluation of guided regularized random forest for classification and regression tasks in remote sensing. Int J Appl Earth Obs Geoinf 88:102051. https://doi.org/10.1016/J.JAG.2020.102051

Jamei E, Chau HW, Seyedmahmoudian M, Stojcevski A (2021) Review on the cooling potential of green roofs in different climates. Sci Total Environ 791:148407. https://doi.org/10.1016/J.SCITOTENV.2021.148407

Jato-Espino D, Manchado C, Roldán-Valcarce A, Moscardó V (2022) ArcUHI: a GIS add-in for automated modelling of the urban heat Island effect through machine learning. Urban Clim 44:101203. https://doi.org/10.1016/J.UCLIM.2022.101203

Joshi MY, Rodler A, Musy M et al (2022) Identifying urban morphological archetypes for microclimate studies using a clustering approach. Build Environ 224:109574. https://doi.org/10.1016/J.BUILDENV.2022.109574

Joshi MY, Teller J (2021) Urban integration of green roofs: current challenges and perspectives. Sustainability 13:12378. https://doi.org/10.3390/SU132212378

Joshi MY, Selmi W, Binard M, et al (2020) Potential for urban greening with green roofs: a way towards smart cities. https://doi.org/10.5194/isprs-annals-VI-4-W2-2020-87-2020

Kim SW, Brown RD (2021) Urban heat island (UHI) variations within a city boundary: a systematic literature review. Renew Sustain Energy Rev 148:111256. https://doi.org/10.1016/j.rser.2021.111256

Kleerekoper L, van Esch M, Salcedo TB (2012) How to make a city climate-proof, addressing the urban heat island effect. Resour Conserv Recycl 64:30–38. https://doi.org/10.1016/j.resconrec.2011.06.004

Kokalj Ž, Somrak M (2019) Why not a single image? Combining visualizations to facilitate fieldwork and on-screen mapping. Remote Sens 11:747. https://doi.org/10.3390/RS11070747

Kontschieder P, Bulò SR, Bischof H, Pelillo M (2011) Structured class-labels in random forests for semantic image labelling. Proc IEEE Int Conf Comp Vis 2190–2197. https://doi.org/10.1109/ICCV.2011.6126496

Li H, Liu Y, Zhang H et al (2021) Urban morphology in China: dataset development and spatial pattern characterization. Sustain Cities Soc 71:102981. https://doi.org/10.1016/j.scs.2021.102981

Li D, Bou-Zeid E, Oppenheimer M (2014) The effectiveness of cool and green roofs as urban heat island mitigation strategies. Environ Res Lett 9. https://doi.org/10.1088/1748-9326/9/5/055002

Lin M, Dong J, Jones L et al (2021) Modeling green roofs' cooling effect in high-density urban areas based on law of diminishing marginal utility of the cooling efficiency: a case study of Xiamen Island, China. J Clean Prod 316:128277. https://doi.org/10.1016/J.JCLEPRO.2021.128277

Lyu F, Wang S, Han SY, et al (2022) An integrated cyberGIS and machine learning framework for fine-scale prediction of Urban Heat Island using satellite remote sensing and urban sensor network data. Urban Inform 1:1–15. https://doi.org/10.1007/S44212-022-00002-4

Matsuki K, Kuperman V, van Dyke JA (2016) The Random Forests statistical technique: an examination of its value for the study of reading. Sci Stud Read 20:20–33. https://doi.org/10.1080/10888438.2015.1107073/SUPPL_FILE/HSSR_A_1107073_SM1111.DOCX

Mirzaei PA (2015) Recent challenges in modeling of urban heat island. Sustain Cities Soc 19:200–206. https://doi.org/10.1016/J.SCS.2015.04.001

Montandon L, Small E (2008) The impact of soil reflectance on the quantification of the green vegetation fraction from NDVI. Remote Sens Environ 112:1835–1845. https://doi.org/10.1016/j.rse.2007.09.007

Razzaghmanesh M, Beecham S, Salemi T (2016) The role of green roofs in mitigating urban heat Island effects in the metropolitan area of Adelaide, South Australia. Urban for Urban Green 15:89–102. https://doi.org/10.1016/J.UFUG.2015.11.013

Rodler A, Leduc T (2019) Local climate zone approach on local and micro scales: dividing the urban open space. Urban Clim 28:100457. https://doi.org/10.1016/j.uclim.2019.100457

Roth M, Oke TR, Emery WJ (1989) Satellite-derived urban heat islands from three coastal cities and the utilization of such data in urban climatology. Int J Remote Sens 10(11):1699–1720

Santamouris M (2013) Energy and climate in the urban built environment. Routledge, London

Stewart ID, Oke TR (2012) Local climate zones for urban temperature studies. Bull Am Meteorol Soc 93:1879–1900. https://doi.org/10.1175/BAMS-D-11-00019.1

USGS (2019) Landsat 8 (L8) Data Users Handbook. USGS, Sioux Falls, South Dakota

Wang X, Li H, Sodoudi S (2022) The effectiveness of cool and green roofs in mitigating urban heat island and improving human thermal comfort. Build Environ 217:109082. https://doi.org/10.1016/J.BUILDENV.2022.109082

Wang B, Geoffroy S, Bonhomme M (2021) Urban form study for wind potential development. 49:76–91. https://doi.org/10.1177/2399808321994449

Wong MS, Nichol JE, To PH, Wang J (2010) A simple method for designation of urban ventilation corridors and its application to urban heat island analysis. Build Environ 45:1880–1889. https://doi.org/10.1016/j.buildenv.2010.02.019

Wu Z, Zhang Y (2018) Spatial variation of urban thermal environment and its relation to green space patterns: implication to sustainable landscape planning. Sustainability 10:2249. https://doi.org/10.3390/SU10072249

Yang J, Bou-Zeid E (2019) Scale dependence of the benefits and efficiency of green and cool roofs. Landsc Urban Plan 185:127–140. https://doi.org/10.1016/J.LANDURBPLAN.2019.02.004

Zakšek K, Oštir K, Kokalj Ž (2011) Sky-view factor as a relief visualization technique. Remote Sensing 3:398–415. https://doi.org/10.3390/RS3020398

Zha Y, Gao J, Ni S (2010) Use of normalized difference built-up index in automatically mapping urban areas from TM imagery. 24:583–594. https://doi.org/10.1080/01431160304987